Inorg. Chem. **2008**, *47*, 8652−8664

Multi-Dimensional Transition-Metal Coordination Polymers of 4,4′-Bipyridine-*N*,*N*′-dioxide: 1D Chains and 2D Sheets

Junhua Jia, Alexander J. Blake, Neil R. Champness,* Peter Hubberstey,* Claire Wilson, and Martin Schröder*

School of Chemistry, University Park, University of Nottingham, Nottingham, NG7 2RD, U.K.

Received March 7, 2008

Reaction of 4,4′-bipyridine-*N*,*N*′-dioxide (L) with a variety of transition-metal salts in MeOH affords a range of coordination polymer products. For the complexes $[FeCl_3(\mu\text{-L})]_\infty$, **1**, and $([Cu(L)_2(OHMe)_2(\mu\text{-L})] \cdot 2PF_6 \cdot n(solv))_\infty$, **2**, 1D chain structures are observed, whereas $([Mn(\mu\text{-L})_3] \cdot 2ClO_4)_\infty$, **3**, and $([Cu(\mu\text{-L})_3] \cdot 2BF_4)_\infty$, **4**, both show 2D sheet architectures incorporating an unusual 3^6-**hxl** topology. The more common 4^4-**sql** topology is observed in $[Cd(ONO_2)_2(\mu\text{-L})_2]_\infty$, **5**, $([Cu(OHMe)_2(\mu\text{-L})_2] \cdot 2ZrF_5)_\infty$, **6**, $([Cu(L)_2(\mu\text{-L})_2] \cdot 2EF_6)_\infty$ (**7** E = P; **8** E = Sb), and $([Et_4N][Cu(OHMe)_{0.5}(\mu\text{-L})_2(\mu\text{-FSiF}_4\text{F})_{0.5}] \cdot 2SbF_6 \cdot n(solv))_\infty$, **9**. In **6**, the $[ZrF_5]^-$ anion, formed in situ from $[ZrF_6]^{2-}$, forms 1D anionic chains $([ZrF_5]^-)_\infty$ of vertex-linked octahedra, and these chains thread through a pair of inclined polycatenated $([Cu(OHMe)_2(\mu\text{-L})_2]^{2+})_\infty$ 4^4-**sql** grids to give a rare example of a triply intertwined coordination polymer. **9** also shows a 3D matrix structure with 4^4-**sql** sheets of stoichiometry $([Cu(L)_2]^{2+})_\infty$ coordinatively linked by bridging $[SiF_6]^{2-}$ anions to give a structure of 5-c $4^4.6^6$-**sqp** topology. The mononuclear $[Cu(L)_6] \cdot 2BF_4$ (**10**) and $[Cd(L)_6] \cdot 2NO_3$ (**11**) and binuclear complexes $[(Cu(L)(OH_2))_2(\mu\text{-L})_2)] \cdot 2SiF_6 \cdot n(solv)$, **12**, are also reported. The majority of the coordination polymers are free of solvent and are nonporous. Thermal treatment of materials that do contain solvent results in structural disintegration of the complex structures giving no permanent porosity.

Introduction

Inorganic−organic coordination frameworks are materials of enormous current interest[1−3] owing to the need not only to understand how crystalline and ordered materials may be engineered[4] but also to elucidate the underlying processes of self-assembly.[5] Furthermore, the rational design and targeted synthesis of multi-dimensional molecular architectures is of significance in the quest for coordination polymers either with solvent-inclusion[6] or gas adsorption[7] characteristics or with electronic[8] or nonlinear optical properties.[9] Using the building-block methodology,[2,10] a range of frameworks has been prepared incorporating cationic centers with linear *N*-donor bidentate bridging ligands such as 4,4′-

* To whom correspondence should be addressed. E-mail: m.schroder@nottingham.ac.uk (M.S.), peter.hubberstey@nottingham.ac.uk (P.H), neil.champness@ nottingham.ac.uk (N.R.C.).

(1) Batten, S. R.; Robson, R. *Angew. Chem., Int. Ed.* **1998**, *37*, 1460–1494.
(2) (a) Blake, A. J.; Champness, N. R.; Hubberstey, P.; Li, W.-S.; Schröder, M.; Withersby, M. W. *Coord. Chem. Rev.* **1999**, *183*, 117–138. (b) Khlobystov, A. N.; Blake, A. J.; Champness, N. R.; Lemenovskii, D. A.; Majouga, A. G.; Zyk, N. V.; Schröder, M. *Coord. Chem. Rev.* **2001**, *222*, 155–192.
(3) Moulton, B.; Zaworotko, M. J. *Chem. Rev.* **2001**, *101*, 1629–1658.
(4) (a) Biradha, K.; Sarkar, M.; Rajput, L. *Chem. Commun.* **2006**, 4169–4179. (b) Sarkar, M.; Biradha, K. *Cryst. Growth Des.* **2007**, *7*, 1318–1331.
(5) (a) Swiegers, G. F.; Malefetse, T. J. *Chem. Rev.* **2000**, *100*, 3483–3538. (b) Seidel, S. R.; Stang, P. J. *Acc. Chem. Res.* **2002**, *35*, 972–983.
(6) (a) Lin, X.; Blake, A. J.; Wilson, C.; Sun, X. Z.; Champness, N. R.; George, M. W.; Hubberstey, P.; Mokaya, R.; Schröder, M. *J. Am. Chem. Soc.* **2006**, *128*, 10745–10753. (b) Zeng, M.-H.; Feng, X.-L.; Chen, X.-M. *Dalton Trans.* **2004**, 2217–2223. (c) Chae, H. K.; Siberio-Pérez, D. Y.; Kim, J.; Go, Y. B.; Eddaoudi, M.; Matzger, A. J.; O'Keeffe, M.; Yaghi, O. M. *Nature* **2004**, *427*, 523–527.
(7) (a) Lin, X.; Jia, J.; Hubberstey, P.; Schroder, M.; Champness, N. R. *CrystEngComm* **2007**, *9*, 438–448. (b) Dinča, M.; Dailly, A.; Liu, Y.; Brown, C. M.; Neumann, D. A.; Long, J. R. *J. Am. Chem. Soc.* **2006**, *128*, 16876–16883. (c) Jia, J.; Lin, X.; Wilson, C.; Blake, A. J.; Champness, N. R.; Hubberstey, P.; Walker, G.; Cussen, E. J.; Schröder, M. *Chem. Comm.* **2007**, 840–842. (d) Chen, B.; Liang, C.; Yang, J.; Contreras, D. S.; Clancy, Y. L.; Lobkovsky, E. B.; Yaghi, O. M.; Dai, S. *Angew. Chem., Int. Ed.* **2006**, *45*, 1390–1393.
(8) (a) Ye, Q.; Song, Y.-M.; Wang, G.-X.; Chen, K.; Fu, D.-W.; Chan, P. W. H.; Zhu, J.-S.; Huang, S. D.; Xiong, R.-G. *J. Am. Chem. Soc.* **2006**, *128*, 6554–6555. (b) Bordiga, S.; Lamberti, C.; Ricchiardi, G.; Regli, L.; Bonino, F.; Damin, A.; Lillerud, K.-P.; Bjorgen, M.; Zecchina, A. *Chem. Commun.* **2004**, 2300–2301.
(9) Zhang, L.-J.; Yu, J.-H.; Xu, J.-Q.; Lu, J.; Bie, H.-Y.; Zhang, X. *Inorg. Chem. Commun.* **2005**, *8*, 638–642.
(10) Rosi, N. L.; Eddaoudi, M.; Kim, J.; O'Keeffe, M.; Yaghi, O. M. *CrystEngComm* **2002**, 401–404.

10.1021/ic800422g CCC: $40.75
Published on Web 08/29/2008

Scheme 1. Anti (a) and syn conformations (b) and double-bridge formation (c) by 4,4′-bipyridine-*N*,*N*′-dioxide coordinated to metal centers, and potential hydrogen-bonding interactions (d)(e) involving coordinated solvent molecules [water (R=H) or methanol (R=Me)][a]

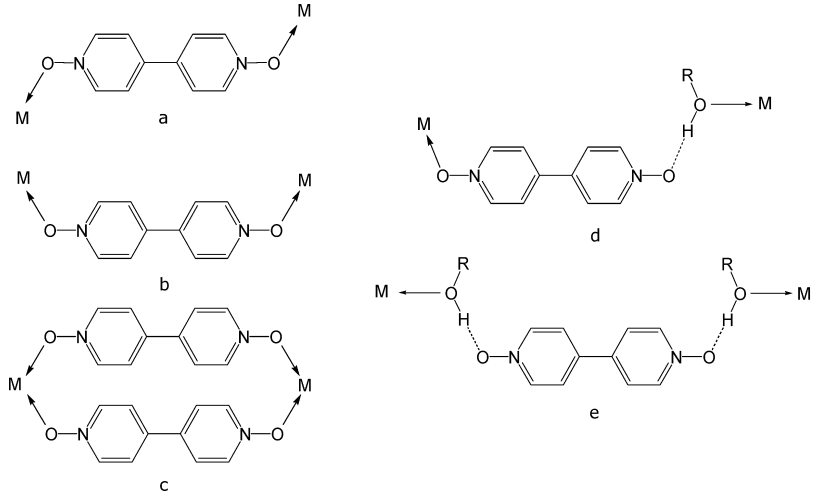

[a] Although syn conformations are shown for the hydrogen-bonding interactions (d, e), anti conformations are equally viable.

bipyridine. Owing to the rigidity of such linkers, the framework architecture in these systems is dictated predominantly by the connectivities and geometries of the metal centers with linear two-connected metal nodes leading to 1D chains, and T-shaped three-connected nodes affording 1D ladders, 2D sheets, and 3D matrices. Four-connected metal nodes can be either square planar or tetrahedral to give 2D sheets or adamantoid cages, respectively, whereas six-connected octahedral metal centers lead to a range of 3D networks.[2,3,11] We have introduced the less sterically demanding and structurally more flexible ligand 4,4′-bipyridine-*N*,*N*′-dioxide (L) and have shown this to be effective for binding hard lanthanide metal ions.[12] 4,4′-Bipyridine-*N*,*N*′-dioxide can bridge metal centers in both anti [part (a) of Scheme 1] and syn conformations [part (b) of Scheme 1] as well as forming double bridges [part (c) of Scheme 1]. Other possibilities are available as the design of framework materials is not solely dependent on the metal center and ligand linker, and the choice of anion and solvent needs to be taken into account as these can bind to metal centers. This reduces the number of coordination sites available for ligand binding and thus reduces both the overall connectivity of the metal center and the dimensionality of the resultant framework. With protic solvent molecules such as water and MeOH, the propensity of the O-donors of 4,4′-bipyridine-*N*,*N*′-dioxide to act as hydrogen-bond acceptors via O−H···O hydrogen bonds with coordinated protonic donors may result in complex hydrogen-bonded supramolecular interactions.[12,13] Thus, metal centers can be bridged by L via direct coordination or via hydrogen bonding to a coordinated protic solvent molecule [parts (d) and (e) of Scheme 1]. Both syn and anti conformations can be envisaged for both possibilities and a competition arises for the *N*,*N*′-dioxide O-centers between metal coordination and hydrogen-bond formation, depending upon the strength of the *N*,*N*′-dioxide oxygen → metal and solvent oxygen → metal coordinate bonds as well as solvent → *N*,*N*′-dioxide O−H···O hydrogen-bonding interactions.

We have used 4,4′-bipyridine-*N*,*N*′-dioxide to bridge a range of lanthanide(III) centers to successfully generate an extensive series of high coordination number and high connectivity framework materials with diverse topologies.[14] We report herein the binding of 4,4′-bipyridine-*N*,*N*′-dioxide to *d*-block metal centers to afford a range of chain and sheet structures. Although several complexes of *d*-block transition-metal centers and 4,4′-bipyridine-*N*,*N*′-dioxide have been reported previously, few form coordinate bonded framework materials.[15−26] Of those which have been described, 1D

(11) Sui, B.; Fan, J.; Okamura, T.; Sun, W.-Y.; Ueyama, N. *Solid State Sci.* **2005**, *7*, 969–982.
(12) (a) Long, D-L.; Blake, A. J.; Champness, N. R.; Schröder, M. *Chem. Commun.* **2000**, 1369–1370. (b) Long, D-L.; Blake, A. J.; Champness, N. R.; Wilson, C.; Schröder, M. *J. Am. Chem. Soc.* **2001**, *123*, 3401–3402. (c) Long, D-L.; Blake, A. J.; Champness, N. R.; Wilson, C.; Schröder, M. *Angew. Chem., Int. Ed.* **2001**, *40*, 2444–2447. (d) Long, D-L.; Hill, R. J.; Blake, A. J.; Champness, N. R.; Hubberstey, P.; Proserpio, D. M.; Wilson, C.; Schröder, M. *Angew. Chem., Int. Ed.* **2004**, *43*, 1851–1854. (e) Hill, R. J.; Long, D-L.; Turvey, M. S.; Blake, A. J.; Champness, N. R.; Hubberstey, P.; Wilson, C.; Schröder, M. *Chem. Commun.* **2004**, 1792–1793. (f) Long, D-L.; Blake, A. J.; Champness, N. R.; Wilson, C.; Schröder, M. *Chem.—Eur. J.* **2002**, *8*, 2026–2033.
(13) Hubberstey, P.; Schröder, M.; Champness, N. R. *J. Solid State Chem.* **2005**, *178*, 2414–2419.
(14) Hill, R. J.; Long, D.-L.; Champness, N. R.; Hubberstey, P.; Schröder, M. *Acc. Chem. Res.* **2005**, *38*, 335–348, and references therein.
(15) Ma, B.-Q.; Gao, S.; Sun, H.-L.; Xu, G.-X. *J. Chem. Soc., Dalton Trans.* **2001**, 130–133.
(16) Ma, B.-Q.; Sun, H.-L.; Gao, S.; Xu, G.-X. *Inorg. Chem.* **2001**, *40*, 6247–6253.
(17) Bruda, S.; Andruh, M.; Roesky, H. W.; Journaux, Y.; Noltmeyer, M.; Rivière, E. *Inorg. Chem. Commun.* **2001**, *4*, 111–114.
(18) Nedelcu, A.; éak, Z.; Madalan, A. M.; Pinkas, J.; Andruh, M. *Polyhedron* **2003**, *22*, 789–794.
(19) Ang, S. G.; Sun, B. W. *Cryst. Growth Des.* **2005**, *5*, 383–386.
(20) Plater, M. J.; Foreman, M. R.; St., J.; Slawin, A. M. Z. *Inorg. Chim. Acta* **2000**, *303*, 132–136.
(21) Manna, S. C.; Zangrando, E.; Drew, M. G. B.; Ribas, J.; Chaudhuri, N. R. *Eur. J. Inorg. Chem.* **2006**, 481–490.
(22) Bourne, S. A.; Moitsheki, L. J. *J. Chem. Crystallogr.* **2007**, *37*, 359–367.
(23) (a) Mantero, D. G.; Neels, A.; Stoeckli-Evans, H. *Inorg. Chem.* **2006**, *45*, 3287–3294. (b) See also Jana, A. D.; Manna, S. C.; Rosair, G. M.; Drew, M. G. B.; Mostafa; G.; Chaudhuri, N. R. *Cryst. Growth Des.* **2007**, *7*, 1365–1372.
(24) Long, D.-L.; Blake, A. J.; Champness, N. R.; Schröder, M. *Chem. Commun.* **2000**, 2273–2274.

Table 1. Structurally Characterized Reaction Products, Starting Materials, and Solvents Used in Their Synthesis

	compound[a]	starting materials	solvent
1D Chains			
1	$[FeCl_3(\mu\text{-L})]_\infty$	$FeCl_3 \cdot 6H_2O$	MeOH
2	$([Cu(L)_2(OHMe)_2(\mu\text{-L})] \cdot 2PF_6 \cdot n(solv))_\infty$	$Cu(NO_3)_2 \cdot 2.5H_2O/KPF_6$	MeOH
2D Sheets (3^6-**hxl** Topology)			
3	$([Mn(\mu\text{-L})_3] \cdot 2ClO_4)_\infty$	$Mn(ClO_4)_2 \cdot 6H_2O$	MeOH
4	$([Cu(\mu\text{-L})_3] \cdot 2BF_4)_\infty$	$Cu(BF_4)_2 \cdot xH_2O$	$MeOH/CH_2Cl_2$
2D Sheets (4^4-**sql** Topology)			
5	$[Cd(ONO_2)_2(\mu\text{-L})_2]_\infty$	$Cd(NO_3)_2 \cdot 4H_2O$	MeOH
6	$([Cu(OHMe)_2(\mu\text{-L})_2] \cdot 2ZrF_5)_\infty$	$Cu(NO_3)_2 \cdot 2.5H_2O/Na_2ZrF_6$	MeOH
7	$([Cu(L)_2(\mu\text{-L})_2] \cdot 2PF_6)_\infty$	$Cu(BF_4)_2 \cdot H_2O/KPF_6$	MeOH
8	$([Cu(L)_2(\mu\text{-L})_2] \cdot 2SbF_6)_\infty$	$Cu(NO_3)_2 \cdot 2.5H_2O/(Et_4N)SbF_6$	MeOH
9	$([Et_4N][Cu(OHMe)_{0.5}(\mu\text{-L})_2(\mu\text{-}FSiF_4F)_{0.5}] \cdot 2SbF_6 \cdot n(solv))_\infty$	$Cu(BF_4)_2 \cdot xH_2O/(Et_4N)SbF_6$	MeOH
Molecular; Mononuclear			
10	$[Cu(L)_6] \cdot 2BF_4$	$Cu(BF_4)_2 \cdot xH_2O$	MeOH
11	$[Cd(L)_6] \cdot 2NO_3$	$Cd(NO_3)_2 \cdot 4H_2O$	MeOH/dmf
Molecular; Binuclear			
12	$[(Cu(L)(OH_2))_2(\mu\text{-L})_2] \cdot 2SiF_6 \cdot n(solv)$	$Cu(BF_4)_2 \cdot xH_2O/CuSiF_6$	MeOH

[a] All metal complexes show octahedral coordination except **1**, which is trigonal bipyramidal.

chains are more common than 2D sheets and 3D matrices. 1D chains are typified by $([M(H_2O)_4(\mu\text{-L})] \cdot 2ClO_4 \cdot 2L)_\infty$ (M = Co,[15] Ni,[15] Cu[15,16] or Zn[15]) (**13**) $([Mn(H_2O)_4(\mu\text{-L})] \cdot 2[Cr(bipy)(ox)_2] \cdot 8H_2O)_\infty$ (**14**),[17] $[Cu(H_2O)(N(CN)_2)_2(\mu\text{-L})])_\infty$ (**15**),[18] $[M(H_2O)_2(\mu\text{-L})(\mu\text{-}C_4H_4O_4)]_\infty$ (M = Mn or Zn) (**16**),[19] $([Cu(\mu\text{-L})(\mu\text{-4,4′-bipyridine})] \cdot 2ClO_4 \cdot L \cdot 2H_2O)_\infty$ (**17**),[16] $[M(hfac)_2(\mu\text{-L})]_\infty$ (M = Co or Cu) (**18**),[20] $[Mn(\mu\text{-L})(\mu\text{-ox})]_\infty$ (**19**),[21] and $[Pb(\mu\text{-L})(\mu\text{-X})_2]_\infty$ (X = Cl, Br, or I) (**20**).[22] These systems comprise alternating metal centers with *N*,*N*′-dioxide ligands in anti conformations. The remaining coordination sites are occupied either by solvent molecules alone (**13**, **14**), a mixture of solvent molecules and anions (**15**, **16**), a mixture of ancillary ligands and anions (**17**), or anions alone (**18**, **19**, **20**). In some cases, non-coordinated *N*,*N*′-dioxide molecules hydrogen-bond to coordinated water molecules to give higher dimensionality supramolecular 2D sheets (**13**), whereas in others either ancillary ligands (4,4′-bipyridine; **17**) or ancillary anions (**19**, **20**) bridge chains to give higher dimensionality 2D sheets.

There is just one example of a 2D sheet and one example of a 3D matrix based on 4,4′-bipyridine-*N*,*N*′-dioxide bridging transition-metal cationic centers. In $([Cu(OH_2)(\mu\text{-L})_2](S_2O_6) \cdot H_2O)_\infty$ (**21**)[23] square pyramidal Cu(II) centers are bridged by *N*,*N*′-dioxide to form a 2D 4^4-**sql** grid, whereas in $([M(\mu\text{-L})_3] \cdot S_2O_6 \cdot 7C_2H_5OH)_\infty$ (M = Co or Ni) (**22**)[23] octahedral metal centers are bridged to form a 3D matrix of 6-c $4^8.6^6.8$-**rob** topology. Previously, our own work in this field has yielded a single compound of 2D sheet construction, $([Zn(L)(OHMe)_2(\mu\text{-L})_{1.5}] \cdot SiF_6 \cdot L \cdot 3MeOH)_\infty$ (**23**),[24] and three compounds with 3D architecture, $([Sc(\mu\text{-L})_3] \cdot 3CF_3SO_3 \cdot 2.7CH_3OH \cdot 3H_2O)_\infty$ (**24**)[25] and $([Sc(\mu\text{-L})_3] \cdot 3X)_\infty$ (X = NO_3 or ClO_4) (**25**)[25] as well as hydrogen-bonded species.[23] In (**23**), octahedral Zn(II) centers are bridged by L to form a 6^3-**hcb** brickwall grid, with the terminal and noncoordinated *N*,*N*′-dioxide molecules involved in $\pi-\pi$ stacking interactions, which convert the 6^3-**hcb** grid into a pseudo-4^4-**sql** grid. The 3D matrix structure of (**24**) is analogous to that of (**22**), whereas in (**25**) octahedral metal centers are bridged by L to form α-Po type structures with 6-c $4^{12}.6^3$-**pcu** topology.

Our experience and that of others suggests the need to avoid aqueous solutions and strongly co-ordinating anions when targeting multidimensional structures based on L with transition-metal cationic centers. Metal cations readily bind water and anions to the exclusion of L, resulting in supramolecular frameworks in which the *N*,*N*′-dioxide forms hydrogen bonds to coordinated water molecules. Consequently, the synthesis of the compounds described herein (Table 1) primarily involves the reaction of L with transition-metal tetrafluoroborate, perchlorate, hexafluorophosphate, and hexafluoroantimonate salts in low molecular weight alcohols. Complexes comprising 1D chains (**1** and **2**), 2D sheets with 3^6-**hxl** topology (**3** and **4**), and 4^4-**sql** topology (**5**, **6**, **7**, **8**, and **9**) have been crystallized and structurally identified, together with three molecular assemblies of which two are mononuclear (**10** and **11**), whereas the third is binuclear (**12**). Although a 3D matrix based solely on coordinated 4,4′-bipyridine-*N*,*N*′-dioxide has not been constructed, **9** has a 3D matrix structure with 4^4-**sql** sheets of stoichiometry $([Cu(L)_2]^{2+})_\infty$ coordinatively linked by bridging $[SiF_6]^{2-}$ anions to give a structure with 5-c $4^4.6^6$-**sqp** topology.

Experimental Section

All chemicals except 4,4′-bipyridine-*N*,*N*′-dioxide were bought from Aldrich Chemical Co. and used as received. Elemental analysis (CHN) was performed by the Nottingham University School of Chemistry Microanalytical Service using a Perkin-Elmer 240B instrument. ^1H NMR spectra were obtained in D_2O and referenced to residual protio solvent using a Bruker DPX

(25) Long, D.-L.; Hill, R. J.; Blake, A. J.; Champness, N. R.; Hubberstey, P.; Wilson, C.; Schröder, M. *Chem.—Eur. J.* **2005**, *11*, 1384–1391.
(26) (a) Bourne, S. A.; Moitsheki, L. J. *CrystEngComm* **2005**, *7*, 674–681. (b) Wang, X.-L.; Qin, C.; Wang, E.-B.; Xu, L. *Eur. J. Inorg. Chem.* **2005**, 3418–3421. (c) Visinescu, D.; Pascu, G. I.; Andruh, M.; Magull, J.; Roesky, H. W. *Inorg. Chim. Acta* **2002**, *340*, 201–206. (d) Ma, B.-Q.; Gao, S.; Sun, H.-L.; Xu, G.-X. *CrystEngComm* **2001**, *3*, 147–151. (e) Blake, A. J.; Brett, M. T.; Champness, N. R.; Khlobystov, A. N.; Long, D.-L.; Wilson, C.; Schröder, M. *Chem. Commun.* **2001**, 2258–2259. (f) Ma, B.-Q.; Sun, H.-L.; Gao, S. *Inorg. Chem.* **2005**, *44*, 837–839. (g) Xu, Y.; Yuan, D.; Xu, Y.; Bi, W.; Zhou, Y.; Hong, M. *Acta Crystallogr., Sect. E* **2004**, *60*, m713-m714.

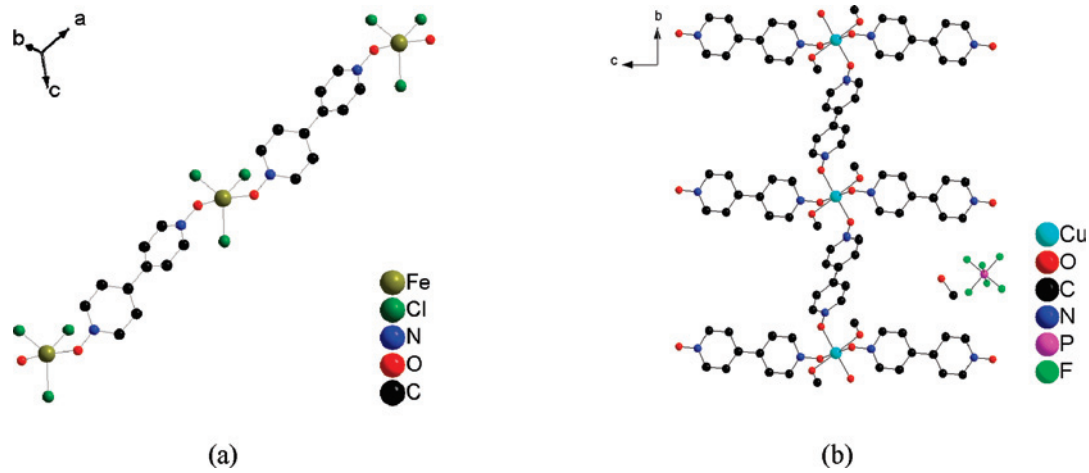

(a) (b)

Figure 1. 1D chains of alternating metal centers and L bridging ligands in **1** (a) and in **2** (b). Hydrogen atoms are omitted for clarity.

Table 2. Structural Parameters Associated with the Bridging L Ligands in the Coordination Polymers **1**−**9**[a]

	complex formula	M−O−N angle/degrees	M···M distances/ angstroms	M−O···O−M torsion angle/degrees	perp. dist. of M from plane of pyridine-*N*-oxide/angstroms	py(1)···py (2) dihedral angle/degrees
1	$[FeCl_3(\mu\text{-L})]_\infty$	122.790(5), 121.973(5)	12.360(1)	164.263(4)	1.509(10),1.720(10)	38.138(1)
2	$([Cu(L)_2(OHMe)_2(\mu\text{-L})]\cdot 2PF_6\cdot n(solv))_\infty$	120.970(9)	12.262(2)	180	1.573(10)	0
		terminal 122.748(9)			1.542(10)	6.604(2)
3	$([Mn(\mu\text{-L})_3]\cdot 2ClO_4)_\infty$	127.942(5), 129.296(8)	12.02(2)	28.94(1)	1.517(10),1.239(10)	24.415(9)
		123.000(8)	12.403(2)	180	1.622(10)	0
4	$([Cu(\mu\text{-L})_3]\cdot 2BF_4)_\infty$	125.926(5), 126.052(3)	11.888(10)	33.870(4)	1.219(10),1.230(10)	28.910(6)
		124.443(5)	12.330(1)	180	1.806(10)	0
5	$[Cd(ONO_2)_2(\mu\text{-L})_2]_\infty$	121.831(4), 121.627(4)	12.2542(7)	36.791(4)	1.549(10),1.616(10)	31.973(5)
6	$([Cu(OHMe)_2(\mu\text{-L})_2]\cdot 2ZrF_5)_\infty$	114.723(8)	11.831(1)	180	0.369(10)	0
		129.168(8)	12.62(2)	180	1.743(10)	0
7	$([Cu(L)_2(\mu\text{-L})_2]\cdot 2PF_6)_\infty$	121.018(11)	12.137(2)	180	1.227(10)	0
		122.834(10)	12.3430(15)	180	1.324(10)	0
		terminal 128.705(9)			1.360(10)	16.186(12)
8	$([Cu(L)_2(\mu\text{-L})_2]\cdot 2SbF_6)_\infty$	123.086(8)	12.185(2)	180	1.360(10)	0
		121.144(10)	12.387(2)	180	1.325(10)	0
		terminal 130.728(8)			1.164(10)	17.977(11)
9	$([Et_4N][Cu(OHMe)_{0.5}(\mu\text{-L})_2(\mu\text{-}FSiF_4F)_{0.5}]\cdot 2SbF_6)_\infty$	117.954(2)	11.9951(4)	180	1.625(10)	0

[a] All metal cations have a formal 2+ charge except for iron in **1**, which has a formal 3+ charge.

Table 3. Selected Interatomic Distances/Angstroms and Angles/Degrees in **1** and **2**[a]

Interatomic distances					
1 Fe−O1	2.0285(13)	Fe−O2	2.0248(13)	Fe−Cl1	2.2502(5)
Fe−Cl2	2.2554(5)	Fe−Cl3	2.2360(6)		
2 Cu−O1	1.990(3)	Cu−O3	1.963(3)	Cu−O4	2.341(3)
Interatomic angles					
1 O2−Fe−O1	166.72(6)	O2−Fe−Cl3	96.49(4)	O1−Fe−Cl3	96.63(4)
O2−Fe−Cl1	90.69(4)	O1−Fe−Cl1	85.71(4)	Cl3−Fe−Cl1	114.63(2)
O2−Fe−Cl2	84.35(4)	O1−Fe−Cl2	88.45(4)	Cl3−Fe−Cl2	114.00(2)
Cl1−Fe−Cl2	131.37(2)				
2 O1−Cu−O3	87.29(12)	O1−Cu−O4	86.88(12)	O3−Cu−O4	90.95(14)

[a] In **2**, the Cu(II) cation is located on a crystallographic inversion center.

300 spectrometer. Single crystals suitable for X-ray diffraction study were taken directly from the reaction media prior to submersion in oil. Samples for elemental analysis were obtained by decantation of supernatant liquid followed by air drying. For those materials that were moisture-sensitive (**2**, **4**, **7**, **8**, **12**), the elemental data conform not to the crystallographically determined structure but to that of the hydrated sample.

Synthesis of 4,4′-bipyridine-*N*,*N*′-dioxide (L). A mixture of 4,4′-bipyridine (0.016 mol, 2.5 g), acetic acid (18 cm^3), and 35% hydrogen peroxide (3.5 cm^3) was heated at 80° for 3 h. An additional portion of hydrogen peroxide (3 cm^3) was added and heating continued for a further 19 h. The solution was then evaporated to dryness in vacuo, and the product recrystallized as colorless needles from hot water (about 5 cm^3) by the addition of large volume of acetone (500 cm^3). Yield: 65% (1.93 g). Analysis: Found (Calcd for $C_{10}H_8N_2O_2$): C, 63.52 (63.81); H, 4.28 (4.29); N, 14.71(14.90)%. ^{1}H NMR (300 MHz, D_2O): $\delta = 7.84$ (4H, d, $J = 9$ Hz), 8.30 (4H, d, $J = 9$ Hz) ppm; $m/z^+ = 189$ (MH^+, 100%); IR (cm^{-1}): 3069(m), 1625(w), 1473(s), 1239(s), 1025(s), 838(s), 547(s).

Synthesis of Metal−Organic Polymers. $[FeCl_3(\mu\text{-L})]_\infty$, 1. $FeCl_3\cdot 6H_2O$ (0.05 mmol, 0.0135 g) and L (0.05 mmol, 0.0094 g) were mixed in MeOH (6 cm^3). Upon slow evaporation at room temperature for 1 week, columnar orange crystals formed at the

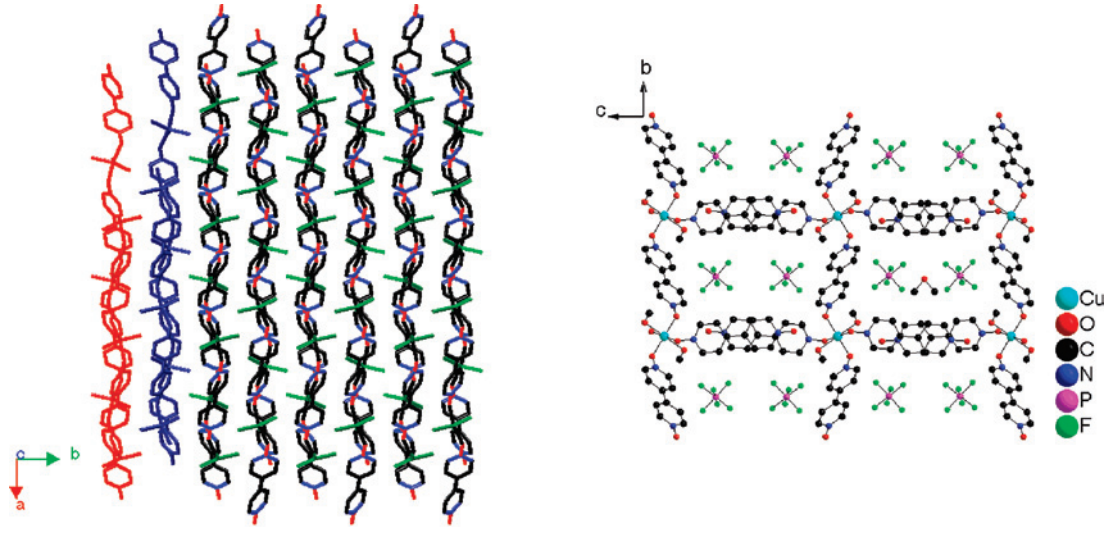

Figure 2. Packing of the 1D chains in **1** (a) and in **2** (b) showing, in the latter case, the formation of the pseudo-4^4-**sql** grid structure via $\pi-\pi$ interactions between pendant L molecules. Hydrogen atoms are omitted for clarity.

Table 4. Selected Inter-Atomic Distances and Angles in **3** and **4** in which the Metals are Located on Crystallographic Inversion Centers[a]

interatomic distances (Å)					
3 Mn−O1	2.1747(15)	Mn−O2	2.1821(15)	Mn−O3	2.1469(14)
4 Cu−O1	1.9761(10)	Cu−O2	1.9740(10)	Cu−O3	2.4075(12)
valence angles (°)					
3 O3−Mn−O1	91.41(6)	O3−Mn−O2[b]	93.83(6)	O1−Mn−O2[c]	94.32(6)
4 O3−Cu−O1	91.42(4)	O3−Cu−O2	95.44(4)	O1−Cu−O2	96.01(4)

[a] $-x, -y, -z$. [b] $x, -y-1/2, z-1/2$. [c] $-x, y+1/2, -z+1/2$.

bottom of the reaction vial (0.0037 g; 0.01 mmol; 21% yield based on L). Analysis: Found (Calcd for $[FeCl_3(L)]_\infty$): C, 34.56 (34.28); H, 2.68 (2.30); N, 7.65 (7.80)%.

$([Cu(L)_2(OHMe)_2(\mu\text{-}L)]\cdot 2PF_6\cdot n(solv))_\infty$, 2. $Cu(NO_3)_2\cdot 2.5H_2O$ (0.05 mmol, 0.0116 g), $K_2TiF_6\cdot 2H_2O$ (0.05 mmol, 0.0120 g), and KPF_6 (0.1 mmol, 0.0184 g) were mixed in MeOH (3 cm^3)and L (0.05 mmol, 0.0094 g) in MeOH (3 cm^3) carefully added. After slow evaporation at room temperature for 1 week, platelike red crystals formed at the bottom of the reaction vial (0.0046 g; 0.0036 mmol; 22% yield based on L). Analysis: Found (Calcd for $([Cu(L)_3(CH_3OH)_2]\cdot 2PF_6\cdot 15H_2O)_\infty$): C, 30.72 (30.69) H, 1.98 (4.99); N, 7.12 (6.71)%.

$([Mn(\mu\text{-}L)_3]\cdot 2ClO_4)_\infty$, 3. $Mn(ClO_4)_2\cdot 6H_2O$ (0.05 mmol, 0.020 g) and L (0.05 mmol, 0.0094 g) were mixed in MeOH (6 cm^3). Upon slow evaporation at room temperature for 1 week, platelike red crystals formed at the bottom of the reaction vial (Yield 0.0026 g; 0.0032 mmol; 19% based on L). Analysis: Found (Calcd for $([Mn(L)_3]\cdot 2(ClO_4))_\infty$): C, 43.66 (44.03); H, 2.96 (2.95); N, 9.96 (10.27)%.

$([Cu(\mu\text{-}L)_3]\cdot 2BF_4)_\infty$, 4. Solid $Cu(BF_4)_2\cdot H_2O$ (0.1 mmol, 0.0232 g) was placed on the bottom of a reaction vial. CH_2Cl_2 (6 cm^3) was added and a solution of L (0.1 mmol, 0.0188 g) in MeOH (6 cm^3) carefully layered over the CH_2Cl_2. Upon slow diffusion at room temperature for 1 week, columnar orange crystals formed at the bottom of the reaction vial (0.0049 g; 0.005 mmol; 15% yield based on L). Analysis: Found (Calcd for $([Cu(L)_3]\cdot 2(BF_4)\cdot 10H_2O)_\infty$): C, 36.92 (36.69); H, 3.25 (4.51); N, 8.56 (8.33)%.

$[Cd(ONO_2)_2(\mu\text{-}L)_2]_\infty$, 5. $Cd(NO_3)_2\cdot 4H_2O$ (0.1 mmol, 0.0308 g) and L (0.05 mmol, 0.0094 g) were mixed in MeOH (10 cm^3). The solution was concentrated to 5 cm^3 and after slow evaporation at room temperature for 1 week, columnar colorless crystals formed at the bottom of the reaction vial (0.002 g; 0.0032 mmol; 13% yield based on L). Analysis: Found (Calcd for $[Cd(L)_2(NO_3)_2]_\infty$): C, 38.29 (39.20); H, 2.56 (2.63); N, 13.19 (13.71)%.

$([Cu(OHMe)_2(\mu\text{-}L)_2]\cdot 2ZrF_5)_\infty$, 6. $Cu(NO_3)_2\cdot 2.5H_2O$ (0.05 mmol, 0.0116 g) and Na_2ZrF_6 (0.05 mmol, 0.0126 g) were mixed in MeOH (3 cm^3), and L (0.05 mmol, 0.0094 g) in MeOH (3 cm^3) was carefully added to the above solution. After slow evaporation at room temperature for 1 week, orange acicular crystals formed at the bottom of the reaction vial (0.0024 g; 0.0027 mmol; 11% yield based on L). Analysis: Found (Calcd for $([Cu(L)_2(CH_3OH)_2]\cdot 2ZrF_5)_\infty$): C, 30.22 (30.14); H, 3.71 (2.76); N, 6.56 (6.39)%.

$([Cu(L)_2(\mu\text{-}L)_2]\cdot 2PF_6)_\infty$, 7. $Cu(BF_4)_2\cdot H_2O$ (0.05 mmol, 0.0120 g) and KPF_6 (0.1 mmol, 0.0184 g) were mixed in MeOH (3 cm^3) and L (0.05 mmol, 0.0094 g) in MeOH (3 cm^3) was carefully added. After slow diffusion at room temperature for 1 week, tabular yellow crystals formed at the bottom of the reaction vial (0.002 g; 0.0016 mmol; 13% yield based on L). Analysis: Found (Calcd for $([Cu(L)_4]\cdot 2PF_6\cdot 10H_2O)_\infty$): C, 37.09 (37.34); H, 2.58 (4.07); N, 8.38 (8.71)%.

$([Cu(L)_2(\mu\text{-}L)_2]\cdot 2SbF_6)_\infty$, 8. $Cu(NO_3)_2\cdot 2.5H_2O$ (0.05 mmol, 0.0116 g) and $(Et_4N)SbF_6$ (0.1 mmol, 0.0366 g) were mixed in MeOH (3 cm^3) and L (0.05 mmol, 0.0094 g) in MeOH (3 cm^3) carefully added. After slow evaporation at room temperature for 1 week, platelike yellow crystals formed at the bottom of the reaction vial (0.0027 g; 0.002 mmol; 16% yield based on L). Analysis: Found (Calcd for $([Cu(L)_4]\cdot 2SbF_6\cdot 4.5H_2O)_\infty$): C, 35.09 (35.10); H, 2.30 (3.01); N, 8.05 (8.18)%.

$([Et_4N][Cu(OHMe)_{0.5}(\mu\text{-}L)_2(\mu\text{-}FSiF_4F)_{0.5}]\cdot 2SbF_6\cdot n(solv))_\infty$, 9. $Cu(BF_4)_2\cdot H_2O$ (0.05 mmol, 0.0120 g) and $(Et_4N)SbF_6$ (0.1 mmol, 0.0366 g) were mixed in MeOH (3 cm^3) and L (0.05 mmol, 0.0094 g) in MeOH (3 cm^3) carefully added. After slow diffusion at room temperature for one week, tabular red crystals formed at the bottom of the reaction vial (0.0022 g; 0.03 mmol; 12% yield based on L). Analysis: Found (Calcd for $([Et_4N][Cu(MeOH)_{0.5}(L)_2(SiF_6)_{0.5}]\cdot 2SbF_6)_\infty$): C, 31.65 (30.22); H, 2.56 (3.26); N, 7.58 (6.29)%.

$[Cu(L)_6]\cdot 2BF_4$, 10. $Cu(BF_4)_2\cdot H_2O$ (0.067 mmol, 0.0156 g) and L (0.2 mmol, 0.0376 g) were dissolved in MeOH (6 cm^3). Upon slow evaporation of the solvent at room temperature for 1 week,

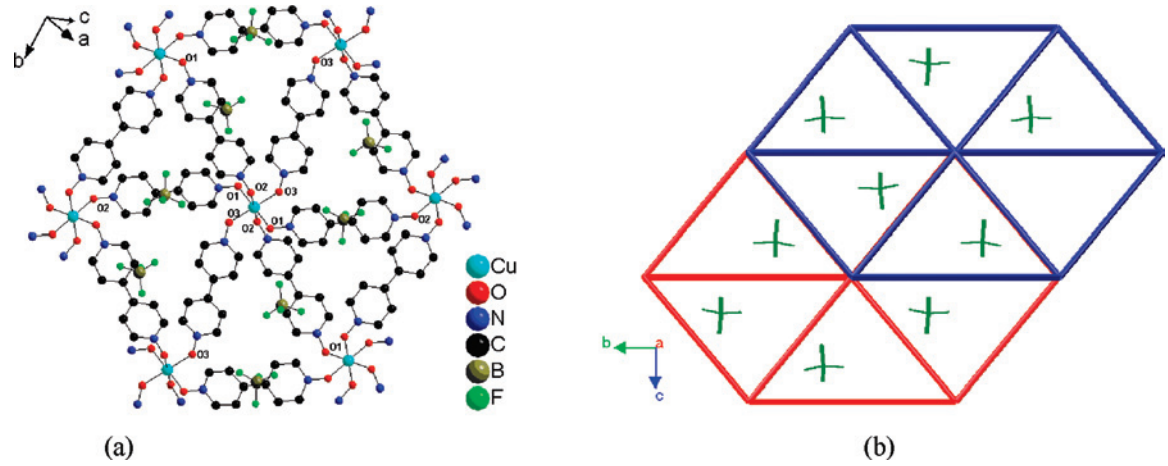

Figure 3. Views of (a) the coordination around the Cu(II) centers and (b) the layers formed in **4**. The AA packing mode is such that layers (red, blue) are stacked directly on top of each other along the *a* axis. Hydrogen atoms in panel a are omitted for clarity.

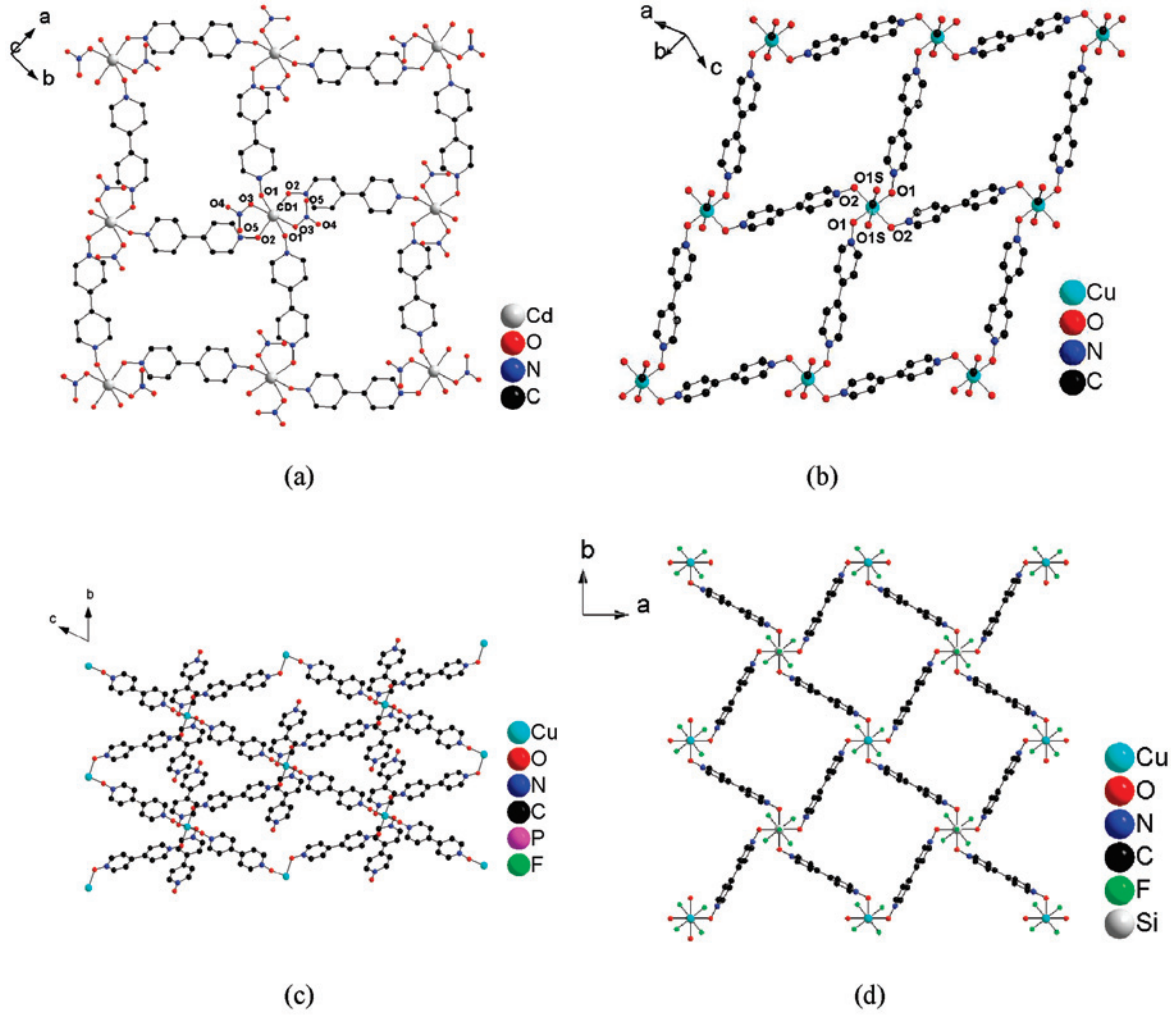

Figure 4. Views of the 4^4 grids in (a) **5**, (b) **6**, (c) **7**, and (d) **9**. Hydrogen atoms are omitted for clarity.

platelike red crystals formed at the bottom of the reaction vial (yield 0.0145 g, 0.0106 mmol, 32% based on L). Analysis: Found (Calcd for $[Cu(L)_6]\cdot 2BF_4$): C, 52.71 (52.74); H, 3.36 (3.54); N, 11.75 (12.30)%.

$[Cd(L)_6]\cdot 2NO_3$, 11. $Cd(NO_3)_2\cdot 4H_2O$ (0.1 mmol, 0.0308 g) and L (0.05 mmol, 0.0094 g) were dissolved in a MeOH /DMF (2:1) solution (5 cm^3) and sealed in a 15 cm^3 bushing type pressure tube. The tube was heated in an oil bath at 100° for 24 h and allowed to cool to room temperature (0.0031 g; 0.0022 mmol; 28% yield based on L). Analysis: Found (Calcd for $[Cd(L)_6]\cdot 2NO_3$): C, 52.94 (52.77); H, 3.36 (3.54); N, 14.48 (14.36)%.

$[(Cu(L)(OH_2))_2(\mu\text{-}L)_2]\cdot 2SiF_6\cdot n$(solv), 12. $Cu(BF_4)_2\cdot H_2O$ (0.05 mmol, 0.0120 g) and $CuSiF_6$ (0.1 mmol, 0.0206 g) were mixed in MeOH (3 cm^3) and L (0.05 mmol, 0.0094 g) in MeOH (3 cm^3) carefully added. Upon slow evaporation at room temperature for one week, light-red platelike crystals formed at the bottom of the

Table 5. Selected Interatomic Distances/Angstroms and Angles/Degrees in **5**−**8** in which the Metals are Located on Crystallographic Inversion Centers

	5 (M═Cd)	**6** (M═Cu)	**7** (M═Cu)	**8** (M═Cu)
M···O1 (L)	2.3052(11)	1.936(2)	1.958(2)	1.954(2)
M···O2 (L)	2.3138(11)	1.931(2)	2.002(2)	2.015(2)
M···O (ax)	2.2912(13)	2.666(3)	2.366(2)	2.363(2)
O1···M···O2	92.25(4)	90.60(8)	90.89(7)	90.72(7)
O1···M···O(ax)	81.11(5)	83.19(8)	88.72(7)	88.11(6)
O2···M···O(ax)	79.33(4)	89.65(8)	84.60(7)	84.30(7)

Table 6. Selected Interatomic Distances/Angstroms and Angles/Degrees in **9** in which the Copper Center Lies on a 4-Fold Rotation Axis

interatomic distances					
Cu···O1	1.930(4)	Cu···F4	2.404(8)	Cu···O(1S)	2.43(4)
interatomic angles					
O1−Cu−O1^a	89.915(13)	O1−Cu−O1^b	175.6(3)	O1−Cu−F2	92.21(16)

^{a} $-y, x, z$. ^{b} $-x, -y, z$.

reaction vial (0.0045 g; 0.0065 mmol; 26% yield based on L). Analysis: Found (Calcd for $[Cu(L)_3(H_2O)_2]\cdot(SiF_6)\cdot 4.5H_2O$): C, 34.22 (34.36); H, 3.46 (4.18); N, 7. 88 (8.01)%.

Crystallography. Single-crystal X-ray diffraction data were collected at 150 K using Bruker SMART CCD area detector diffractometers equipped with Oxford Cryosystems open flow cryostats[27] for all complexes. All data were collected using graphite monochromated Mo Kα radiation (λ = 0.71073 Å). Absorption corrections were performed by multiscan methods.[29] Pertinent details of crystal data, data collection, and processing are given in Table 9. Thermal ellipsoid plots (50% probability) for the asymmetric units of all 12 compounds are included in the Supporting Information (Figure S1). All structures were solved using direct methods using *SHELXS 97*,[28] with the exception of **7** and **8**, which were solved using Patterson methods. All non-hydrogen atoms were located using subsequent Fourier difference methods.[29] In all cases, carbon-bound and coordinated solvent hydrogen atoms were placed in calculated positions and thereafter allowed to ride on their parent atoms. The hydrogen atoms of the disordered MeOH solvent in **2**, of the coordinated and solvate water molecules and solvate methanol molecules in **12**, and the hydrogen atoms of the coordinated MeOH molecule in **9** could not be located. For **11**, a disordered nitrate anion was modeled in two parts with refined occupancies in the ratio 0.689(6):0.311(6). For **12**, twinning by 180 degree rotation about [100] was identified and the frameset integrated using two orientation matrices: twin law (1 0 0.28/0 −1 0/ 0 0 −1) and the value of R_{int} quoted in Table 9 refers to one component. For **8**, one of the fluorine atoms of the $[SbF_6]^-$ anion was disordered over two positions with half-occupancy for each and geometric restraints were applied. For **9**, four fluorine atoms from the $[SbF_6]^-$ anion were each disordered over two positions with occupancies of 0.47 and 0.53, and one fluorine atom from the $[SiF_6]^-$ anion was disordered over two positions with occupancies of 0.6 and 0.4. All of these atoms together with the carbon and oxygen atoms from the coordinated MeOH molecule and $[Et_4N]^+$ cation were refined isotropically.

Free-solvent accessible volumes of 9.0%, 7.6%, 10.9%, 2.6%, and 11.1% were calculated for **12**, **2**, **6**, **5**, and **9**, respectively, by the SOLV module of *PLATON*.[30] For **12**, **2**, **6**, and **9**, the *SQUEEZE* result from *PLATON*[31] corresponded to 29e/Cu, 14e/Cu, 25e/Cu, and 33.5e/Cu, which account for $2.9H_2O$/Cu, $1.4H_2O$/Cu, $2.5H_2O$/Cu, and 0.6MeOH/Cu, respectively. However, the solvent content may vary for different batches of samples. For **5**, no electron density except that in the framework was found confirming that no solvent was held in the micropore. The formulae of the complexes were determined by combining the results of single-crystal X-ray experiment and elemental analysis.

Results and Discussion

Compound Synthesis. A standard synthetic protocol was used for the preparation of the majority of the coordination polymers. A solution of L in MeOH was carefully layered onto a solution of the appropriate transition-metal salt in MeOH, and, if required, a salt of an additional non-coordinating anion. Product crystals appeared following slow evaporation at room temperature. In the presence of KPF_6, $(Et_4N)SbF_6$, or $CuSiF_6$, $Cu(BF_4)_2\cdot H_2O$ gave **7**, **9**, and **12**, respectively, whereas in the absence of a second added anion $[Cu(L)_6]\cdot 2BF_4$, **10**, was isolated. It is interesting to note that **9** contains the $[SiF_6]^{2-}$ dianion, formed in situ by reaction of BF_4^-, water, and the glass vessel, in preference to the BF_4^- anion. In the presence of KPF_6, Na_2ZrF_6, or $(Et_4N)SbF_6$, reaction of $Cu(NO_3)_2\cdot 2.5H_2O$ with L yielded **2**, **6**, and **8**, respectively. It is interesting to note that the formation of **6** involves the conversion of the molecular $[ZrF_6]^{2-}$ anion into the $([ZrF_5]^-)_\infty$ anion, which forms a 1D chain structure based on vertex-sharing octahedra. Under the same conditions and in the absence of any other anion, $Mn(ClO_4)_2\cdot 6H_2O$ gave **3**, whereas $FeCl_3.6H_2O$ and $Cd(NO_3)_2\cdot 4H_2O$ gave **1** and **5** respectively.

4 and **11** were obtained in modified experiments. Columnar orange crystals of **4** were isolated following slow diffusion at room temperature of a system comprising CH_2Cl_2 layered above solid $Cu(BF_4)_2\cdot xH_2O$ with a methanolic solution of L carefully layered above. Colorless tabular crystals of **11** were extracted from the mixture remaining after a MeOH/dmf (2:1) solution containing $Cd(NO_3)_2\cdot 4H_2O$ and L had been heated in a sealed pressure tube to 100° for 24 h.

Coordination Polymers Based on 1D Motifs. The basic architectural feature of **1** and **2** is a 1D chain of alternating metal centers and molecules of L [parts (a) and (b) of Figure 1], which adopt an anti conformation [part (a) of Scheme 1, Table 2]. The approximate trigonal bipyramidal geometry at the Fe(III) center in **1** is completed by three chloride anions [Table 3], whereas the tetragonally elongated distorted octahedral geometry at the Cu(II) center in **2** is completed by two pairwise pendant L molecules and two MeOH molecules [Table 3, part (b) of Figure 1].

The chains in **1** pack in a parallel fashion along the *a* axis [part (a) of Figure 2] and are weakly linked by aromatic C−H···Cl hydrogen-bonds. The chains in **2** align along the *b* axis such that the non-coordinated O-centers of pendant *N*,*N*′-dioxide from adjacent chains act as hydrogen-bonding acceptors to coordinated methanol OH groups (O···O 2.688

(27) Cosier, J.; Glazer, A. M. *J. Appl. Crystallogr.* **1986**, *19*, 105–107.
(28) Sheldrick, G. M. *SHELXS 97 and SHELXL 97*; University of Göttingen: Göttingen, Germany, 1997.
(29) Sheldrick, G. M. *TWINABS*, University of Göttingen: Göttingen, Germany, 2004.
(30) Spek, A. L. *J. Appl. Crystallogr.* **2003**, *36*, 7–13.
(31) Sluis, P. van der.; Spek, A. L. *Acta Crystallogr., Sect. A* **1991**, *46*, 194–201.

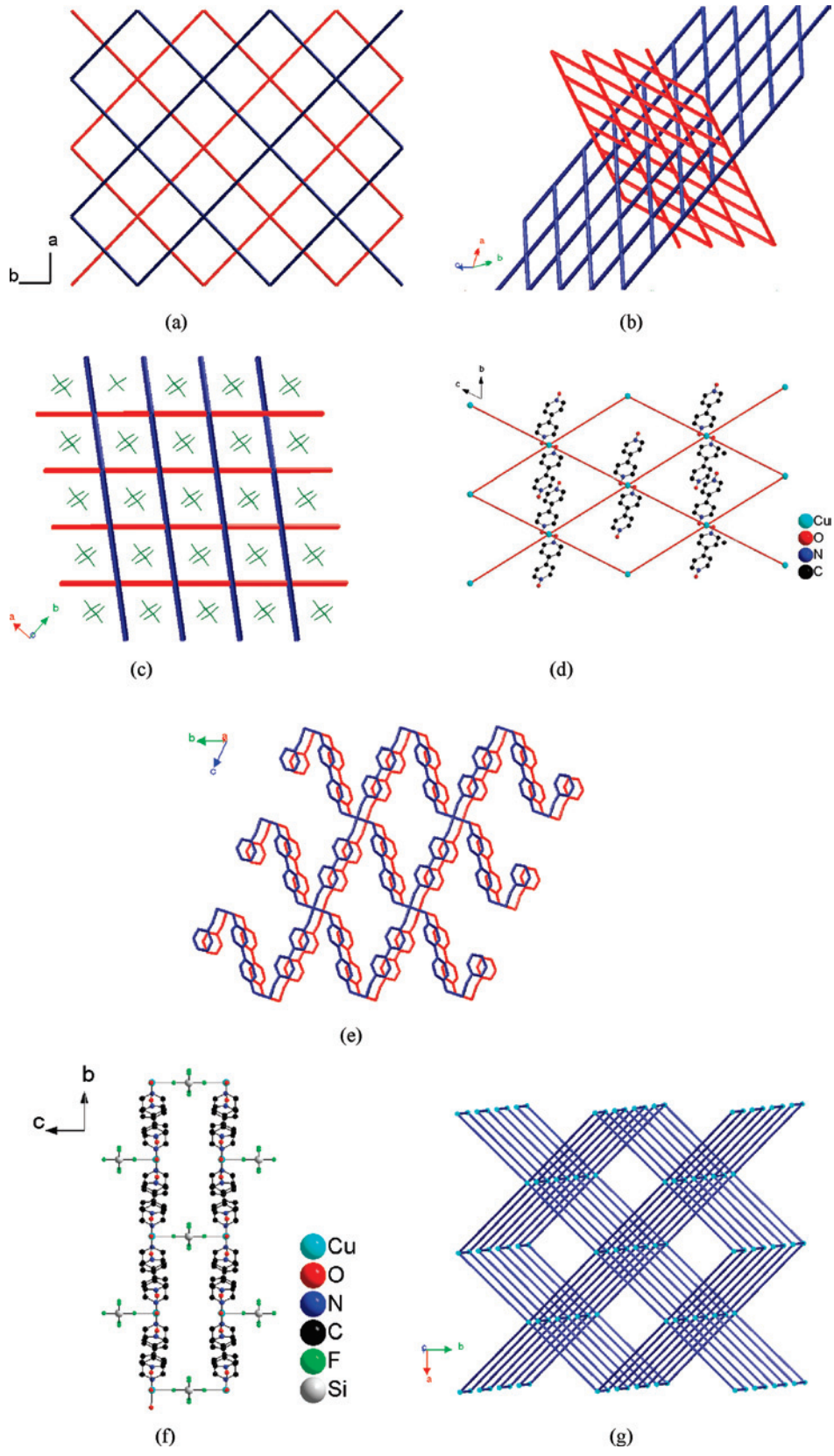

Figure 5. A view of the structure of **5** showing (a) the AB packing mode of the 4^4-**sql** connected layers. Views of the structure of **6** showing (b) the polycatenation of the layers and (c) the occupation by counterions of the channels running parallel to the *c* axis. Views of the structure of **7** perpendicular to the (1 0 0) plane showing (d) the aromatic face-to-face $\pi-\pi$ stacking interaction and (e) the channels occupied by counterions. Views of the structure of **9** perpendicular to the (1 0 0) and (0 0 1) planes showing (f) the linking of the 4^4-**sql** sheets by the $[SiF_6]^{2-}$ anions and (g) the 3D matrix of 5-c $4^4.6^6$-**sqp** topology. The 4^4-**sql** grids are shown in simplified form in (a−d, g). The pendant *N*,*N*′-dioxide molecules from (e), the axial MeOH molecules from (g), and the hydrogen atoms from (d-f) are omitted for clarity.

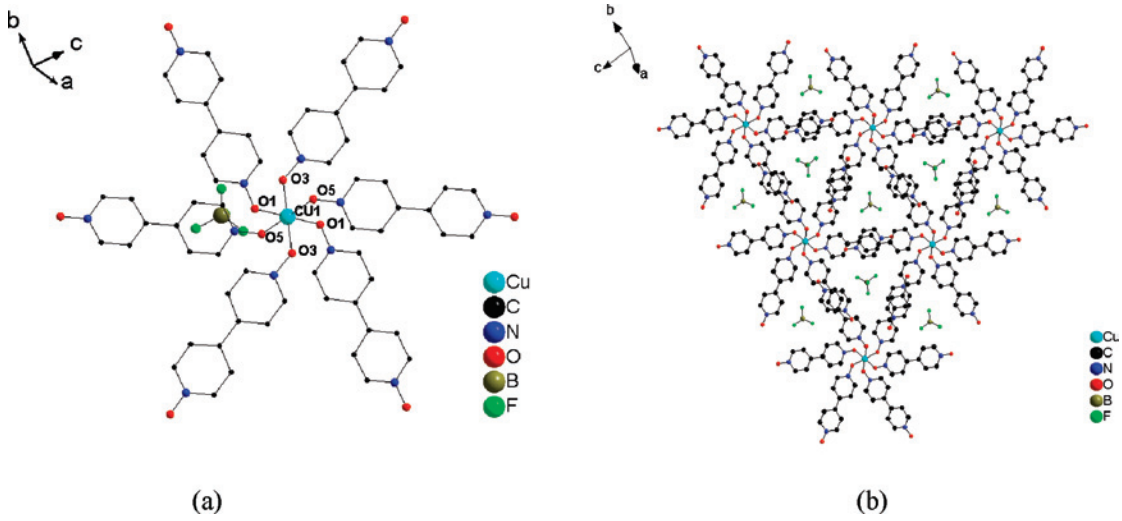

(a) (b)

Figure 6. Views of **10** showing (a) the coordination of the Cu(II) center and (b) the packing of the molecular $[Cu(L)_6]^{2+}$ cations by aromatic face-to-face $\pi-\pi$ stacking interactions to give a 2D sheet structure of bilayer appearance with pseudo 3^6-**hxl** topology. Hydrogen atoms are omitted for clarity.

Table 7. Selected Inter-Atomic Distances and Angles in **10**, **11**, and **26** in which the Metals are Located on Crystallographic Inversion Centers

coordination sphere; interatomic distances					
10 Cu−O1	1.9759(12)	Cu−O3	1.9790(12)	Cu−O5	2.3151(13)
11 Cd−O1	2.2844(14)	Cd−O3	2.2508(13)	Cd−O5	2.2303(13)
26 Zn−O1	2.109(3)	Zn−O3	2.081(2)	Zn−O5	2.063(3)
coordination sphere; interatomic angles					
10 O1−Cu−O3	89.42(5)	O1−Cu−O5	84.30(5)	O3−Cu−O5	84.99(5)
11 O1−Cd−O3	84.74(5)	O1−Cd−O5	94.92(5)	O3−Cd−O5	90.70(5)
26 O1−Zn−O3	93.46(10)	O1−Zn−O5	86.54(10)	O3−Zn−O5	90.51(10)

intrabilayer interactions; distances and angles	perpendicular separation/Å	centroid−centroid/Å	offset angle/°
10 $[Cu(L)_6]\cdot 2BF_4$	3.27−3.28	3.510(1), 3.654(1), 3.519(1)	82.63(1), 79.65(1), 73.37(1)
11 $[Cd(L)_6]\cdot 2NO_3$	3.38−3.42	3.546(1), 3.647(1), 3.543(1)	75.56(1), 78.75(1), 74.11(1)
26 $[Zn(L)_6]\cdot 2NO_3$	3.28−3.40	3.517(1), 3.612(1), 3.508(1)	78.35(2), 80.40(2), 74.99(2)
interbilayer interactions; distances and angles			
10 $[Cu(L)_6]\cdot 2BF_4$	3.27−3.47	3.456(1), 3.456(1), 3.625(1)	70.09(1), 75.68(1), 69.61(1)
11 $[Cd(L)_6]\cdot 2NO_3$	2.84−3.71	3.489(1), 3.489(1), 3.741(1)	85.70(1), 67.99(1), 63.34(1)
26 $[Zn(L)_6]\cdot 2NO_3$	3.08−3.87	3.461(1), 3.541(1), 3.664(1)	84.85(2), 80.20(2), 66.63(2)

Table 8. Selected Interatomic Distances/Angstroms and Angles/Degrees in **12**

interatomic distances					
Cu−O1	2.185(7)	Cu−O3	1.987(7)	Cu−O4	1.969(7)
Cu−O1W	1.955(7)	Cu−O2W	1.961(7)		
interatomic angles					
O3−Cu−O1	99.2(3)	O4−Cu−O1	92.7(3)	O2W−Cu−O1	94.1(3)
O1W−Cu−O1	83.0(3)	O4−Cu−O3	92.7(3)	O2W−Cu−O3	166.3(3)
O1W−Cu−O3	88.7(3)	O2W−Cu−O4	90.2(3)	O1W−Cu−O4	175.6(3)
O1W−Cu−O2W	89.3(3)				

Å) to form a 3D net with 4-c $6^5.8$-**cds** 2-fold topology within which all of the edges down [0 0 1] are double-bridged hydrogen bonds [part (b) of Figure 2]. Aromatic, face-to-face $\pi-\pi$ stacking interactions between the pendant *N*,*N*′-dioxide molecules [perpendicular separation = 3.41−3.58 Å; centroid−centroid distance = 4.0371(5) Å; offset angle = 60.086(5)°] support the formation of the 3D grid.

Coordination Polymers Based on 2D Motifs. 3^6-hxl Nets. In **3** and **4**, each six-coordinate distorted octahedral metal center (Table 4) is connected to six crystallographically related metal centers through bridging 4,4′-bipyridine-*N*,*N*′-dioxide linkers [part (a) of Figure 3], two of which adopt an anti-coordination [part (a) of Scheme 1, Table 2] with the remainder adopting a syn conformation [part (b) of Scheme 1, Table 2] to form a 2D grid of 3^6-**hxl** topology [part (b) of Figure 3]. Such grids are still rare with only six examples having been previously described.[32] Selected interatomic distances and angles for **3** and **4** are summarized in Table 4. The ligands L are arranged around the metal centers to give approximately D_{3d} local symmetry, although the Cu(II) center in **4** is subject to a Jahn−Teller distortion typical of d^9 electronic configurations. The layers are stacked along the *a* axis in an eclipsed arrangement through aromatic face-to-face $\pi-\pi$ stacking interactions to give triangular channels in which the counteranions (**3**, ClO_4^-; **4**, BF_4^-) are located [part (b) of Figure 3]; for **3**, perpendicular separation = 3.17−4.37 Å; centroid−centroid distances = 3.9605(4), 3.8292(4), 3.7905(4) Å; offset angles = 51.638(5), 76.932(4), 78.695(4)°; for **4**, perpendicular separation = 3.19−4.27 Å;

(32) (a) Williams, C. A.; Blake, A. J.; Hubberstey, P.; Schröder, M. *Chem. Commun.* **2005**, 5435–5437. (b) Du, M.; Jiang, X.-J.; Zhao, X.-J. *Inorg. Chem.* **2007**, *46*, 3984–3995. (c) Edgar, M.; Mitchell, R.; Slawin, A. M. Z.; Lightfoot, P.; Wright, P. A. *Chem.—Eur. J.* **2001**, 5168–5175. (d) Burrows, A. D.; Cassar, K.; Friend, R. M. W.; Mahon, M. F.; Rigby, S. P.; Warren, J. E. *CrystEngComm* **2005**, *7*, 548–550. (e) Hawxwell, S. M.; Adams, H.; Brammer, L. *Acta Crystallogr.* **2006**, *B62*, 808–814. (f) Su, C.-Y.; Cai, Y.-P.; Chen, C.-L.; Kang, B.-S. *Inorg. Chem.* **2001**, *40*, 2210–2211.

Table 9. Crystal Data and Structure Refinement for Transition-Metal 4′-bipyridine-*N*,*N*′-Dioxide **1**−**12**

complex	**1**	**2**	**3**	**4**	**5**	**6**
empirical formula	$[Fe(L)Cl_3]_\infty$	$([Cu(L)_3(OHMe)_2]\cdot 2PF_6\cdot n(solv))_\infty$	$([Mn(L)_3]\cdot 2ClO_4)_\infty$	$([Cu(L)_3]\cdot 2BF_4)_\infty$	$([Cd(L)_2(NO_3)_2])_\infty$	$([Cu(L)_2(OHMe)_2]\cdot 2ZrF_5)_\infty$
fw	350.38	1014.16	818.39	801.71	612.79	876.43
T/K	150(2)	150(2)	150(2)	150(2)	150(2)	150(2)
cryst syst	monoclinic	monoclinic	monoclinic	monoclinic	monoclinic	monoclinic
space group	$P2_1/n$	$P2/c$	$P2_1/c$	$P2_1/c$	$P2_1/c$	$C2/c$
a/Å	12.3596(12)	7.0131(11)	8.4318(12)	8.3593(8)	9.1248(8)	19.569(2)
b/Å	9.1961(9)	10.059(2)	12.403(2)	12.3297(11)	16.8177(15)	13.306(2)
c/Å	12.5172(12)	28.818(5)	15.087(2)	15.0316(14)	7.4667(7)	13.617(2)
α/°	90	90	90.00	90.00	90.00	90.00
β/°	115.162(1)	90.711(3)	99.970(3)	100.566(2)	105.095(1)	128.647(2)
γ/°	90	90	90.00	90.00	90.00	90.00
V/Å^3	1287.7(4)	2032.8(10)	1554.0(6)	1523.0(4)	1106.3(3)	2769(1)
Z	4	2	2	2	2	4
D_{calcd}(g/cm^3)	1.807	1.657	1.749	1.748	1.840	2.102
absorption coefficient	1.786	0.731	0.683	0.824	1.060	1.614
reflns collected	14 310	10 536	9029	13 825	9776	8568
independent reflns	2946 [*R*(int) = 0.023]	3645 [*R*(int) = 0.035]	3545 [*R*(int) = 0.024]	3663 [*R*(int) = 0.017]	2521 [*R*(int) = 0.012]	3155 [*R*(int) = 0.025]
GOF on F^2	1.04	1.08	1.036	1.06	1.04	0.93
final *R* indexes [$I > 2\sigma(I)$]	0.0260	0.0595	0.0344	0.0298	0.0187	0.0315
wR_2 (all data)	0.0666	0.158	0.0808	0.0781	0.0462	0.0661
largest diff. peak/hole (eÅ^{-3})	0.45/−0.22	0.76/−0.49	0.48/−0.31	0.46/−0.18	0.36/−0.24	0.81/−0.58

complex	**7**	**8**	**9**	**10**	**11**	**12**
empirical formula	$([Cu(L)_4]\cdot 2PF_6)_\infty$	$([Cu(L)_4]\cdot 2SbF_6)_\infty$	$([Et_4N][Cu(OHMe)_{0.5}(\mu\text{-}L)_2(\mu\text{-}FSiF_4F)_{0.5}]\cdot 2SbF_6\cdot n(solv))_\infty$	$[Cu(L)_6]\cdot 2BF_4$	$[Cd(L)_6]\cdot 2NO_3$	$[(Cu(L)(OH_2))_2(\mu\text{-}L)_2]\cdot 2SiF_6\cdot n(solv)$
fw	1106.22	1287.78	1147.95	1366.26	1365.52	668.09
T/K	150(2)	150(2)	150(2)	150(2)	150(2)	150(2)
cryst syst	triclinic	triclinic	tetragonal	triclinic	triclinic	monoclinic
space group	$P\bar{1}$	$P\bar{1}$	$I4/m$	$P\bar{1}$	$P\bar{1}$	$P2_1/c$
a/Å	8.719(1)	9.039(1)	16.9501(8)	8.8698(10)	8.8749(13)	17.955(4)
b/Å	11.616(2)	11.397(1)	16.9501(8)	11.5176(13)	11.779(2)	7.275(2)
c/Å	12.137(2)	12.185(2)	15.3669(14)	14.167(2)	13.969(2)	19.454(4)
α/°	62.571(2)	63.270(2)	90.00	104.558(2)	104.179(2)	90
β/°	76.607(2)	75.425(2)	90.00	96.540(2)	95.648(2)	98.758(4)
γ/°	76.515(2)	77.368(2)	90.00	99.413(2)	98.822(2)	90
V/Å^3	1049.9(4)	1076.9(4)	4415(1)	1363.6(3)	1384.9(6)	2512(2)
Z	1	1	4	1	1	4
D_{calcd}(g/cm^3)	1.750	1.986	1.727	1.664	1.637	1.767
absorption coefficient	0.716	1.851	1.809	0.510	0.488	1.019
reflns collected	8710	9500	2624	12 383	12 190	9658
independent reflns	4665 [*R*(int) = 0.022]	4866 [*R*(int) = 0.018]	2619 [*R*(int) = 0.019]	6144 [*R*(int) = 0.023]	6244 [*R*(int) = 0.015]	6257 [*R*(int) = 0.067]
GOF on F^2	1.02	1.03	1.11	1.04	1.07	1.19
final *R* indexes [$I > 2\sigma(I)$]	0.0464	0.0296	0.0870	0.0366	0.0312	0.0711
wR_2 (all data)	0.108	0.0770	0.251	0.0952	0.0811	0.214
largest diff. peak/hole (eÅ^{-3})	0.56/−0.30	1.57/−0.63	2.37/−1.44	0.41/−0.33	0.92/−0.20	0.77/−0.70

centroid−centroid distances = 3.7473(3), 3.7427(3), 3.7343(3) Å; offset angles, 78.750(3), 71.907(3), 77.787(3)°.

4^4-sql nets. 2D Grids of 4^4-**sql** topology comprising 4-connected metal nodes and bridging *N*,*N*′-dioxide molecules are the principal architectural feature of **5**, **6**, **7**, **8**, and **9** (Figure 4). In each complex four *N*,*N*′-dioxide ligands are bound to the metal center at the equatorial sites of six-coordinate distorted octahedral centers (**5**−**9**). The axial coordination sites are occupied by either NO_3^- anions [**5**; part (a) of Figure 4], MeOH molecules [**6**; part (b) of Figure 4] or pendant *N*,*N*′-dioxide molecules [**7** and **8**; part (c) of Figure 4], whereas those at the Cu(II) center in **9** are occupied by a $[SiF_6]^{2-}$ anion and a slightly more remote MeOH solvent molecule. Selected interatomic distances and angles are collected in Tables 5 and 6. The bridging *N*,*N*′-dioxide ligands generally adopt an anti conformation [part (a) of Scheme 1, Table 2], the exception being those in **5** and **9** which adopt a syn conformation [part (b) of Scheme 1, Table 2]. Owing to the restricted space available within the structure of **9**, only one MeOH molecule can be modeled between two copper centers.

The 4^4-**sql** grids pack in these compounds in a number of different ways to give extended structures. In **3**, the layers align along the *a* axis in a staggered arrangement through aromatic face-to-face $\pi-\pi$ stacking interactions [perpendicular separation = 3.50−3.69 Å, centroid-centroid distance = 3.8741 Å; offset angle = 88.676°) to give an AB packing mode with the axially located NO_3^- anions interdigitated in the center of the rectangular cavities of adjacent sheets [part (a) of Figure 5]. In **6**, the sheets polycatenate with a dihedral angle of 82.1(1)°, as shown in parts (b) and (c) of Figure 5. This arrangement gives rise to diamondoid shaped channels, which run parallel to the *c* axis and which are occupied by 1D chains of $([ZrF_5]^-)_\infty$ anions [part (c) of Figure 5] to give

a triply intertwined motif. This architecture is quite exceptional, owing to the rarity of not only triply intertwined motifs[33] but also polycatenation and polythreading involving different polymeric motifs.[34]

In **7** and **8**, the 2D sheets are aligned parallel such that terminal *N*,*N*′-dioxide ligands from adjacent sheets form aromatic face-to-face $\pi-\pi$ stacking interactions [for **7**, perpendicular separation = 3.26−3.29 Å; centroid−centroid distance = 3.9585(6) Å; offset angle = 59.666(7)°; for **8**, perpendicular separation, = 3.35−3.39 Å; centroid−centroid distance = 3.8609(3)Å; offset angle = 61.741(6)°] to give a 3D matrix architecture [parts (d) and (e) of Figure 5]. This arrangement gives rise to channels directed along the *b* axis, which are occupied by the $[EF_6]^-$ anions (E = P or Sb). The architecture in **9** involves 2D sheets linked by bridging bidentate $[SiF_6]^{2-}$ anions to give a pillared layered structure, stacked along the *c* axis, as shown in part (f) of Figure 5. The topology of the 3D extended structure of **9** based on a five-connected metal center and linear *N*,*N*′-dioxide and $[SiF_6]^{2-}$ linkers is 5-c $4^4.6^6$-**sqp** [part (g) of Figure 5] with square channels running along the *c* axis and occupied by the second counterion $[SbF_6]^-$.

Molecular Species. Three novel molecular species were obtained during the course of this work. **10** and **11** are mononuclear, whereas the third (**12**) is binuclear. The mononuclear species are analogous to $[Zn(L)_6]\cdot 2NO_3$ (**26**), the first example of an octahedral metal center coordinated by six 4,4′-bipyridine-*N*,*N*′-dioxide ligands [Figure 6].[24] Each metal cation occupies a crystallographic inversion center, which results in three crystallographically independent ligands. The pyridyl rings within each of these ligands are twisted with respect to each other with dihedral angles ranging from 15.33 to 27.64°. The six ligands are distributed alternately in two parallel planes around the metal center so that the cation has approximate D_{3d} symmetry [part (a) of Figure 6]. Whereas the Zn(II) and Cd(II) metal centers are virtually symmetrical with M···O distances in the limited ranges [Zn, 2.063−2.109 Å; Cd, 2.251−2.285 Å], the Cu(II) center exhibits tetragonal elongation typical of Jahn−Teller distorted d^9 systems [Cu−O, 1.976, 1.979, 2.315 Å]. Selected interatomic distances and angles in **10**, **11**, and **26** are listed in Table 7. The $[M(L)_6]^{2+}$ moieties interact through face-to-face $\pi-\pi$ contacts involving the uncoordinated pyridine *N*-oxide rings of the *N*,*N*′-dioxide to form 2D sheets [part (b) of Figure 6]. These sheets, which have a pseudobilayer appearance, are of 3^6-**hxl** topology, and the intrabilayer interatomic distances and angles for the stacking interactions for the three complexes are summarized in Table 7. The sheets align in an eclipsed fashion along the *a* axis through aromatic face-to-face $\pi-\pi$ stacking interactions to give an AAA packing motif within which there are triangular channels occupied by the counterions [part (b) of Figure 6]. The interbilayer interatomic distances and angles for the stacking interactions for the three complexes are summarized in Table 7.

The binuclear complex **12** comprises a centrosymmetric $[Cu_2(L)_4(H_2O)_4]^{4+}$ cationic unit, $[SiF_6]^{2-}$ anions, and MeOH molecules. Selected interatomic distances and angles are listed in Table 8. Within each $[Cu_2(L)_4(H_2O)_4]^{4+}$ moiety [part (a) of Figure 7], two *N*,*N*′-dioxide molecules, both of which adopt syn conformations, bridge the Cu(II) centers [part (c) of Scheme 1], the five-coordinate square pyramidal coordination geometries of which are completed by a terminal *N*,*N*′-dioxide ligand and two water molecules. The aromatic rings of the *N*,*N*′-dioxide bridges are also involved in intracation aromatic face-to-face $\pi-\pi$ stacking interactions [perpendicular separation = 3.11−3.60 Å; centroid−centroid distance = 3.466(1) Å; offset angle = 88.016(9)°] with two bridging *N*,*N*′-dioxide ligands and two water molecules located in the cis position in the square base, Cu−O = 1.955(7) and 1.987(7) Å. This leaves a terminal *N*,*N*′-dioxide ligand located at an apical position, Cu−O = 2.185(7) [part (a) of Figure 7]. The terminal *N*,*N*′-dioxide ligands act as hydrogen-bond acceptors to water O−H donors [O···O 2.5792(6), 2.6297(5) Å] coordinated to adjacent $[Cu_2(L)_4(H_2O)_4]^{4+}$ units [part (d) of Scheme 1], thus forming zigzag chains aligned along the [1 0 1] direction [part (b) of Figure 7]. An intercation aromatic face-to-face $\pi-\pi$ interaction between the pyridine rings of the terminal *N*,*N*′-dioxide ligands [perpendicular separation = 3.56−3.96 Å; centroid−centroid distance = 3.660(1) Å; offset angle = 86.727(9)°] supports the formation of a zigzag chain. The $[SiF_6]^{2-}$ counter-ions and solvent MeOH molecules reside in the spaces between the chains, which are stacked along the *c* axis [part (c) of Figure 7]. They are locked in position by hydrogen-bond formation with coordinated water molecules [O···F (coordinated H_2O to SiF_6^{2-} anion) = 2.5863(5) Å; (solvent methanol to SiF_6^{2-} anion) = 2.7504(4) Å; part (c) of Figure 7]. The structure of the supramolecular chain in **12** is highly reminiscent of that in the structure of $[Zn_2(3,3'\text{-pytz})_3(MeOH)_2(NO_3)_4]$ (3,3′-pytz = 3,6-bis(pyridine-3-yl)-1,2,4,5-tetrazine),[35] in which the binuclear molecular unit comprising two centrosymmetrically related [Zn(3,3′-pytz)(OHMe)$(ONO_2)_2$] moieties bridged by a single 3,3′-pytz molecule is linked into a supramolecular 1D chain through methanol···3,3′-pytz O−H···N hydrogen-bonds. The two chains differ solely in the number of bridging molecules within the binuclear unit and the supramolecular hydrogen-bonding motif.

Thermal Stability. The majority of the products obtained in this work crystallize free of solvent and hence are nonporous. Of those that contain solvent, **6** and **9** contain MeOH bound to Cu(II), whereas **12** contains uncoordinated MeOH locked in place by hydrogen-bonding to coordinated *N*,*N*′-dioxide and $[SiF_6]^{2-}$ counteranions. All of the products are unstable with rapid structural collapse when the sample is exposed to air. Disintegration can be clearly observed under a microscope.

(33) Biradha, K.; Fujita, M. *Chem. Commun.* **2002**, 1866–1867.
(34) (a) Carlucci, L.; Ciani, G.; Proserpio, D. M. *New J. Chem.* **1998**, *22*, 1319–1321. (b) Hagrman, P.; Hagrman, D.; Zubieta, J. *Angew. Chem., Int. Ed.* **1999**, *38*, 2638–2684.
(35) Withersby, M. A.; Blake, A. J.; Champness, N. R.; Cooke, P. A.; Hubberstey, P.; Li, W.-S.; Schröder, M. *Inorg. Chem.* **1999**, *38*, 2259–2266.

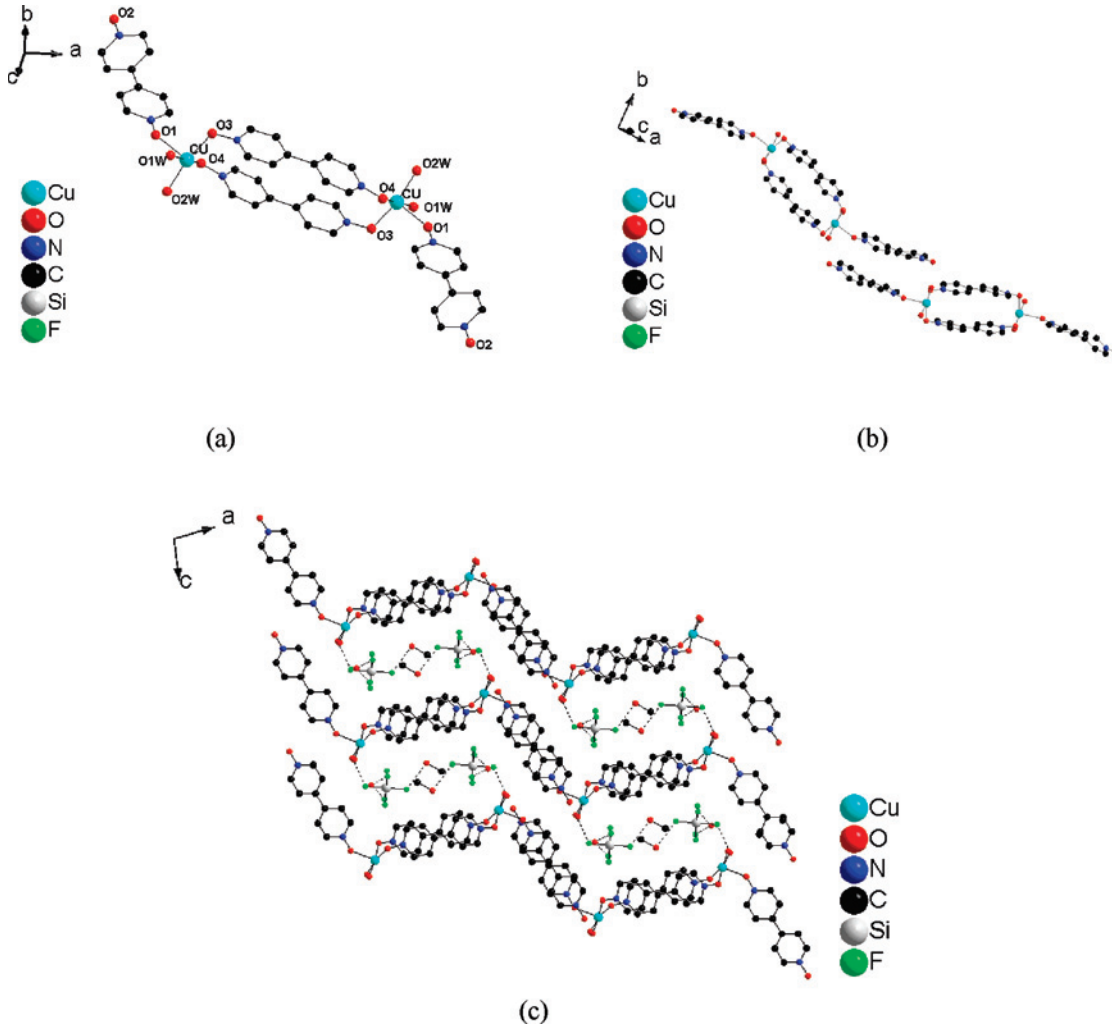

Figure 7. Views of **12** showing (a) the coordination of the Cu(II) center in the $[Cu_2(L)_4(H_2O)_4]^{4+}$ unit, (b) the aromatic face-to-face $\pi-\pi$ stacking interaction to give zigzag chains oriented along the [1 0 1] direction, and (c) the packing of the zigzag chains. Hydrogen atoms are omitted for clarity.

For those materials that are air-stable, structural collapse is confirmed after TGA analysis by PXRD of the resultant amorphous materials. Thus, none of these materials show permanent porosity. For the moisture-sensitive materials (**2**, **4**, **7**, **8**, **12**), the elemental analytical data conform not to the crystallographically determined structure but to a hydrated sample.

Conclusions

By using MeOH as the solvent for synthesis, it has proven possible to form a variety of coordination polymers in which metal centers [Mn(II) **3**, Fe(III) **1**, Cu(II) **2**, **4**, **6**−**9**, and Cd(II) **5**] are bridged by 4,4′-bipyridine-*N*,*N*′-dioxide to construct 1D chains (**1** and **2**) and 2D sheets of either 3^6-**hxl** (**4** and **3**) or 4^4-**sql** topology (**5**−**9**). Although no 3D matrices solely bridged by L have been produced, **9** is a 3D coordination polymer with 4^4-**sql** grids linked by bridging $[SiF_6]^{2-}$ anions to give an architecture with 5-c $4^4.6^6$-**sqp** topology. Despite the use of hydrated transition-metal salts as starting materials, which gives a methanol−water reaction media, few of the products have coordinated MeOH and only **12** has coordinated water. Presumably, the weaker coordinating ability of MeOH and the reduced chemical potential of water in the solvent mixture allow preferential coordination by *N*,*N*′-dioxide molecules and the formation of coordination polymers.

The construction of 2D sheets with both 3^6-**hxl** and 4^4-**sql** topologies is directly attributable to the flexible coordination geometry of the ligating oxygen atoms of L. Such variety would be unlikely with rigid linear ligands such as 4,4′-bipyridine, which often leads to products where the coordination preferences of the metal center determine and dominate architecture type. The flexibility of the ligand L is manifest in the range of observed M···M separations (11.83−12.62 Å, Table 2).

Of the 14 crystallographically independent bridging *N*,*N*′-dioxide molecules in these products, 10 lie across inversion centers and thus adopt the anti conformation (M−O···O−M torsion angle = 180°, Table 2) with parallel pyridine *N*-oxide rings (dihedral angle = 0°, Table 2). Of the remaining four bridging *N*,*N*′-dioxide molecules, one adopts the anti conformation (M−O···O−M torsion angle = 164.26°, Table 2) and three adopt the syn conformation (M−O···O−M torsion angle = 28.9−36.8°, Table 2). Interestingly, all of these *N*,*N*′-dioxide molecules are twisted at the C4−C4′ bond (maximum dihedral angle

= 38.1°), and the metal cations are not coplanar with the pyridine *N*-oxide ring to which they are bonded. The perpendicular distance of the cation from the plane of the pyridine *N*-oxide ring varies from 1.164 to 1.806 Å with just one exception − that in **6**, which is only 0.369 Å distant. Also, the range of M−O−N angles is rather wide in this series of complexes (<M−O−N = 115−130°, average = 123.7°, Table 2), suggesting that it is the steric requirements of the metal center rather than electronic effects of the ligand itself that determine the position of the metal relative to the pyridine *N*-oxide ring.

Stoichiometric variation has been achieved in, (i) the Cu(II)−L−$[BF_4]^-$ system, with compounds containing Cu/L ratios of 1:3 (**4**) and 1:6 (**10**) being obtained from layering and evaporation experiments, respectively, (ii) the Cd(II)−L−$[NO_3]^-$ system with compounds containing Cd/L ratios of 1:2 (**5**) and 1:6 (**11**) being obtained from evaporation and solvothermal experiments, respectively, and, (iii) the Cu(II)−L−$[PF_6]^-$ system, with compounds containing Cu/L ratios of 1:3 (**2**) and 1:4 (**7**) being obtained from $[NO_3]^-$ and $[BF_4]^-$ precursors, respectively. Structural variety has also been achieved by the introduction of ancillary anions ($[SiF_6]^{2-}$ (**12**), $[PF_6]^-$ (**2** or **7**), $[SbF_6]^-$ (**8** or **9**) or $([ZrF_5]^-)_\infty$ (**6**)) in the Cu(II)−L−$[BF_4]^-$ and Cu(II)−L−$[NO_3]^-$ systems. Even in the absence of an added ancillary anion, the formation of a particular structure is so favored that the equilibrium associated with the hydrolysis of the $[BF_4]^-$ anion:

$$[BF_4]^- + H_2O \leftrightarrow [B(OH)F_3]^- + HF \quad (1)$$

is disturbed to such an extent that a Cu(II)−L−$[SiF_6]^{2-}$ coordination polymer (**9**) is produced following fluoride attack of the Pyrex vessel. A similarly promoted transformation occurs in the crystallization of **6** from the Cu(II)−L−$[BF_4]^-$/$[ZrF_6]^{2-}$ system, when the molecular $[ZrF_6]^{2-}$ anion is converted into the fluoride-bridged 1D $([ZrF_5]^-)_\infty$ anion.

With the exception of **9**, none of the products form 3D structures. Owing to the effective packing of 1D chains and 2D sheets as well as molecular species, most of the products are nonporous with only **2**, **9**, and **12** containing limited accessible volume. However, the structures of **2**, **9**, and **12** do not survive removal of coordinated solvent, and the products do not show permanent porosity. Nonetheless, we are investigating the formation of porous materials using unusual ligand tectons and are concentrating on the synthesis of novel extended bidentate bridging *N*,*N*′-dioxides as well as branched multidentate analogues.

Acknowledgment. This work was supported by Engineering and Physical Science Research Council (EPSRC), the University of Nottingham and the CVCP (ORS award to J.J.). M.S. gratefully acknowledges receipt of a Royal Society Wolfson Merit Award and of a Leverhulme Trust Senior Research Fellowship.

Supporting Information Available: X-ray crystallographic data in the form of a CIF file. This material is available free of charge via the Internet at http://pubs.acs.org.

IC800422G